Journal of Hazardous Materials 177 (2010) 516–523

Contents lists available at ScienceDirect

Journal of Hazardous Materials

journal homepage: www.elsevier.com/locate/jhazmat

Influence of calcination on the adsorptive removal of phosphate by Zn–Al layered double hydroxides from excess sludge liquor

Xiang Cheng[a,*], Xinrui Huang[a], Xingzu Wang[b], Dezhi Sun[b]

[a] School of Municipal & Environmental Engineering, Harbin Institute of Technology, 202 Haihe Road, 150090 Harbin, China
[b] College of Environmental Science & Engineering, Beijing Forestry University, 35 Tsinghua East Road, 100083 Beijing, China

ARTICLE INFO

Article history:
Received 15 July 2009
Received in revised form 25 October 2009
Accepted 14 December 2009
Available online 24 December 2009

Keywords:
Calcination
Phosphate adsorption
Sludge liquor
Zn–Al layered double hydroxides

ABSTRACT

The influence of calcination of Zn–Al layered double hydroxides (LDHs) on their phosphate adsorption capacity was studied in order to improve phosphorus removal from an excess sludge liquor. Powder X-ray diffraction (XRD), Fourier transform infrared (FTIR) spectroscopy, scanning electron microscopy (SEM), thermogravimetry-differential scanning calorimetry (TG-DSC) and nitrogen adsorption–desorption were employed to characterize the raw Zn–Al and the calcined products. The results reveal that the Zn–Al LDHs evolved to a phase of mixed metal oxides with the calcination temperature increasing to 300 °C and finally to spinel $ZnAl_2O_4$ at 600 °C. When the Zn–Al was calcined at 300 °C, the interlayer carbonate ions were removed and the greatest BET surface area of 81.20 m^2/g was achieved. The tested phosphate adsorption capacities of the raw and calcined Zn–Al were closely related to the evolution of physicochemical properties of the LDHs during the calcination. The Zn–Al-300 (Zn–Al LDHs calcined at 300 °C) exhibited the highest P uptake of 41.26 mg P/g in 24 h. The phosphate adsorption by the raw Zn–Al and the Zn–Al-300 both follows a pseudo-second-order kinetic model; the adsorption isotherms show a good fit with a Langmuir-type equation.

1. Introduction

Layered double hydroxides (LDHs), also known as hydrotalcite-like compounds or anionic clays, have attracted considerable attention in recent years due to their application as precursors for heterogeneous catalysts [1], electrode surface modifiers [2], anion adsorbents [3–5] and new functional materials [6]. Their general formula can be expressed as $[M^{2+}_{1-x}M^{3+}_x(OH)_2][A^{n-}]_{x/n}\cdot yH_2O$, where M^{2+} and M^{3+} represent di- and tri-valent metal cations, A^{n-} is the intercalated anion and x normally ranges from 0.17 to 0.33 [7]. The high charge density of the sheets from the isomorphic substitution of M^{2+} by M^{3+} and the exchangeability of interlayer anions make LDHs excellent and cheap adsorbents for removing anion pollutants from aqueous environments [3–5].

Phosphate removal from waste streams has been extensively studied and put into practice since people realized that the excess input of phosphorus would accelerate eutrophication of the receiving waters [8,9]. The widely applied methods include chemical precipitation and crystallization [10,11], enhanced biological phosphorus removal (EBPR) processes [12], constructed wetlands [13] and adsorption [14–16]. Adsorptive removal of phosphorus from wastewaters is a cost-effective and environment-friendly technology, by which the chemical sludge production is small and the adsorbed P can be easily recovered. The main challenge for this method is to find or develop a material with a high adsorption capability. Researchers have investigated many different adsorbents, such as industrial byproducts [15], minerals [17], metal oxides/hydroxides [18], ion exchange resins [19], etc.

LDHs have been studied in recent years to remove phosphorus from simple electrolytes [20–24], seawater [25], drain effluents [16], etc. The phosphate adsorption capacity of LDHs varied significantly due to their great diversity in metal precursors, intercalated anions, and preparation methods [21,25,26]. A great number of studies were performed to explore the influencing factors of the adsorption capability of LDHs [27]. Many of the authors reported that calcination markedly improved the anions uptake by LDHs [4,5,25]. The improvement was extensively explained by the rehydration of the calcined LDHs in water, "memory effect", and the increased specific surface area after calcination. However, the relationship among the treatment conditions, the structure of resulted LDHs and their adsorptive properties of anions, especially phosphate, has not been addressed in detail as needed. The mechanisms of phosphate adsorption onto calcined LDHs, therefore, are still not clear.

In the present work, we examined the phosphate adsorption by a raw Zn–Al and the Zn–Als calcined at different temperatures. The structural evolution of the LDHs during the calcination was studied to help explain the variation of phosphate adsorption capacity of

* Corresponding author. Tel.: +86 10 6233 6596; fax: +86 10 6233 6596.
E-mail address: sean.d.cheng@gmail.com (X. Cheng).

0304-3894/$ – see front matter © 2009 Elsevier B.V. All rights reserved.
doi:10.1016/j.jhazmat.2009.12.063

the resulted Zn–Al and subsequently to explore the mechanisms of the phosphate uptake. Sludge liquor from a municipal wastewater treatment was used as the P-rich stream due to its potential for large-scale P recovery in the future.

2. Materials and methods

2.1. Preparation of raw and calcined Zn–Al LDHs

Zn–Al layered double hydroxides were synthesized by coprecipitation method. A 200-mL solution of mixed chloride containing 0.5 M Zn^{2+} and 0.25 M Al^{3+} was prepared in a 500-mL beaker. Under magnetic stirring at 80 °C in a high-purity N_2 atmosphere, the pH of the mixture was adjusted to 9.0 ± 0.2 by dropwise adding 20% NaOH. The resulted slurry was aged at the same temperature for 18 h, then filtered and washed thoroughly with deionized water. The precipitate was dried at 80 °C overnight and ground to ~100-mm particles. The obtained Zn–Al LDHs were calcined at different temperatures from 150 to 600 °C in high-purity nitrogen for 4 h, denoted as Zn–Al-*T*, where *T* stands for the calcination temperature.

2.2. Adsorbent characterization

Chemical analyses for Zn and Al in the synthesized Zn–Al LDHs were conducted by an inductively coupled plasma optical emission spectrometry (ICP-OES) system (Optima 5300DV, PerkinElmer) after dissolving the samples in 0.5 M HCl solutions. Thermogravimetry-differential scanning calorimetry (TG-DSC) measurements of the LDHs were carried out on a NETZSCH STA449C instrument. 4.675 mg of the raw Zn–Al was heated up to 1000 °C (10 °C/min) in an Ar atmosphere at a flow rate of 30 mL/min. Powder X-ray diffraction (XRD) analyses of the samples were conducted using a Rigaku X-ray diffractometer (D/Max-RB) with Cu*Kα* radiation (λ = 1.5418 Å) at 45 kV and 45 mA. XRD patterns were collected over a 2*θ* from 10° to 90° with a scan rate of 5° (2*θ*)/min. Fourier-transform infrared (FIIR) spectra were taken using a PerkinElmer Spectrum one FTIR in the wavenumber range of 400–4000 cm^{-1}. The samples in powder form were mixed with dried KBr powders at 1/99 ratio and pressed into specimens for spectra collection. The surface morphology of the Zn–Al LDHs was identified by scanning electron microscopy (HITACHI S4700). Samples were coated with gold (~20 nm) before observation. The surface area, total pore volume and pore size were measured by the N_2 adsorption–desorption isotherm and Barrett–Joyner–Halenda (BJH) method on an ASAP 2020 instrument (Micromeritics) after the powder sample was outgassed overnight under vacuum (10^{-5} Torr) at 80 °C.

2.3. Phosphate adsorption onto Zn–Al LDHs

The P adsorption capacities of the Zn–Al LDHs and the calcined products were estimated by batch assays in a thermostatic shaker at room temperature. 0.02 g of sample was added into 50 mL of sludge liquor in 117-mL serum bottles. The sludge liquor was from Taiping municipal wastewater treatment plant in Harbin, China (the water composition shown in Table 1). After 24 h of contact (almost equilibrate according to our previous study), the supernatant was filtered through a 0.45-μm membrane and the residual P concentration was measured by the molybdate blue method [28]. LDHs-free controls were performed to observe the non-adsorption degradation of phosphate in the sludge liquor. Kinetics of P adsorption was investigated using the raw Zn–Al and the Zn–Al-300 as the adsorbents. 0.1 g of LDHs sample was added to 250 mL of sludge liquor, and the soluble phosphate concentration was monitored for 72 h. Adsorption isotherms were obtained by mixing known amounts of adsorbents with 250 mL of sludge liquor and testing the equilibrium phosphate concentrations after 72 h of contact at room temperature. All the adsorption assays were performed in triplicate.

Table 1
Characteristics of the sludge liquor.

Parameter	Sludge filtrate
pH	6.80 ± 0.00
SS, mg/L	3.82 ± 0.00
COD, mg/L	514.62 ± 6.24
PO_4^{3-}, mg-P/L	20.00 ± 4.10
NO_2^-, mg/L	ND[a]
NO_3^-, mg/L	ND[a]
SO_4^{2-}, mg/L	112.53 ± 0.42
Cl^-, mg/L	81.44 ± 0.50
NH_4^+, mg/L	84.34 ± 4.82
Na^+, mg/L	83.65 ± 0.19
K^+, mg/L	44.66 ± 0.05
Al^{3+}, mg/L	0.06 ± 0.00
Ca^{2+}, mg/L	105.80 ± 0.60
Cu^{2+}, mg/L	ND[a]
Fe, mg/L	0.24 ± 0.00
Mg^{2+}, mg/L	27.22 ± 0.09
Mn^{2+}, mg/L	1.34 ± 0.01
Zn^{2+}, mg/L	0.01 ± 0.00

[a] ND: non-detectable.

3. Results and discussion

3.1. Characterization of the Zn–Al and the calcined products

Zn–Al layered double hydroxides were synthesized as illustrated by XRD patterns with the characteristic reflection peaks for (0 0 3) and (0 0 6) planes (Fig. 1). The pattern could be indexed to a hexagonal cell (*a* = 3.081 Å and *c* = 23.405 Å). The tested Zn/Al molar ratio (1.94:0.97) corresponded approximately to that in the starting metal solution, indicating an efficiently coprecipitation. Additional

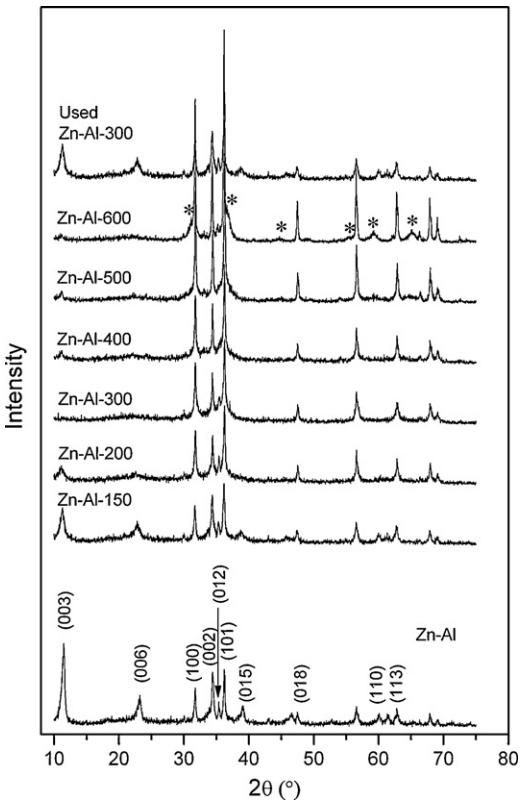

Fig. 1. X-ray diffractograms of the raw Zn–Al and the calcined Zn–Al samples at different temperatures. (*) $ZnAl_2O_4$.

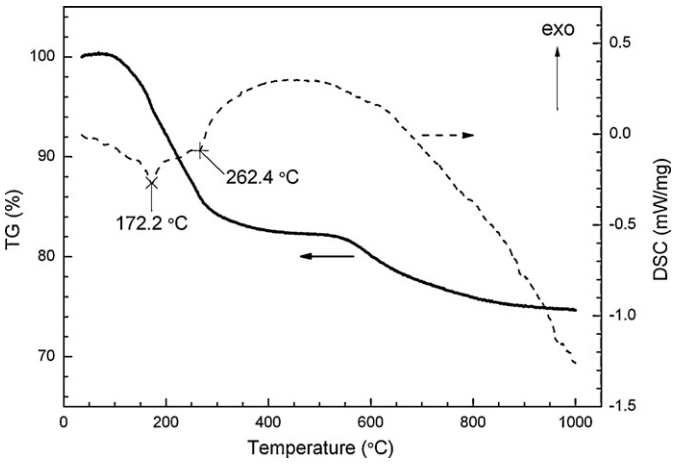

Fig. 2. TG/DSC thermal analysis of the synthesized Zn–Al LDHs.

ZnO phase was present as indicated by the reflections from (1 0 0), (0 0 2) and (1 0 1) planes. The XRD pattern evolution resulting from calcination treatment agrees with the results in previous structural studies of LDHs [29,30]. The layered structure of Zn–Al was preserved at 150 and 200 °C but the crystallinity was lowered as attested by the broadening of the lines and the decrease in their intensities. LDHs phase diminished and was replaced by ZnO phase when the temperature was 300 °C. Spinel phase ($ZnAl_2O_4$) appeared when the temperature increased to 600 °C.

The thermal behavior of the Zn–Al samples was analyzed through TG-DSC experiments. The major mass loss of 17.09% was observed in the temperature range of 80–371 °C (Fig. 2). In the DSC curve, two endothermic peaks were detected correspondingly in this temperature range. The first peak at 172.2 °C is mostly due to the release of the adsorbed and interlayer water, and the second at 262.4 °C is associated with the removal of H_2O and CO_2 from the collapse and dehydroxylation of the metal hydroxide layers [29].

In a FTIR spectrum of the Zn–Al, a broad band centered at ~3469 cm^{-1} (H1 in Fig. 3) was observed, which is due to the stretching mode of hydroxyl groups (ν_{O-H}), both in the brucite-like layers and from the interlamellar water molecules. The broadness of the band indicates that hydrogen bonds with a wide range of strength existed [31]. With the increase in the calcination temperature, the intensity of the OH band was lowered revealing that water molecules were continuously removed from the LDHs during the calcination. A shoulder was observed at ~3444 cm^{-1} (H2 in Fig. 3) when the temperature went beyond 300 °C. This suggests that the remained OH groups were experiencing a restricted environment due to the collapse of the LDHs layers [30].

The band at 1370 cm^{-1} (C1 in Fig. 3) is assigned to the ν_3 (asymmetric stretching mode) of the carbonate anions. The mode at ~1480 cm^{-1} (C2 in Fig. 3) is attributed to the splitting of the ν_3 of the carbonate. Even though there was no carbonate used for the LDHs preparation, some CO_2 in the air would have dissolved into the mixture during the NaOH addition. Upon calcination, the ν_3 mode diminished and lost the intensity at 300 °C, indicating the release of CO_3^{2-} during the thermal treatment.

Three sharp peaks at 674, 548 and 495 cm^{-1} (S1–S3 in Fig. 3) were observed in the spectrum of the Zn–Al-600, which are attributed to the stretching mode of Al–O in an octahedral coordination state (AlO_6 octahedral units). The result suggests the transformation of the crystal phase to spinel $ZnAl_2O_4$ and is in good agreement with the XRD data.

SEM micrographs of the Zn–Al and the Zn–Al-*T* were shown in Fig. 4. A layered structure was observed in the raw Zn–Al. Upon calcination, the whole layer started to break to smaller

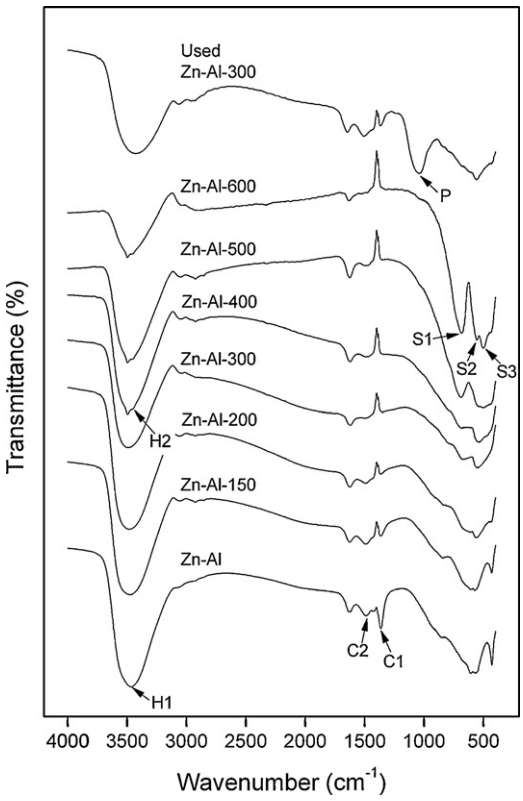

Fig. 3. FTIR spectra of the raw Zn–Al, the calcined Zn–Al at different temperatures and the used Zn–Al-300.

pieces and pores appeared due to the loss of water and anions. When the calcination temperature was higher than 300 °C, the sample sintering occurred. This can be explained by the transformation from the mixed metal oxides to the spinel $ZnAl_2O_4$. These observations were further demonstrated by the analyses of pore structure and surface area of the samples. Fig. 5 shows the nitrogen adsorption–desorption isotherms of the Zn–Al and the calcined products. All the isotherms are type III-like with a distinct H1 hysteretic loop in the range of 0.6–1.0 P/P_0, suggesting the presence of mesoporous materials according to IUPAC classification [32]. The corresponding pore size distribution of the samples was determined by using the Barrett–Joyner–Halenda (BJH) method from the desorption branch of the isotherms (summarized in Table 2). Two stages can be identified for the profile of the average pore size: a decrease with the calcination temperature increased to 300 °C and an increase in the calcination temperature range of 300–600 °C. The BET surface area of the Zn–Al then evolved in the opposite way, obtaining the highest value of 81.20 m^2/g at 300 °C. In terms of the pore volume of the particles, the lowest ones were observed at 300 °C (0.15 cm^3/g) and 600 °C (0.14 cm^3/g), respectively. The former was probably because of the collapse of the layered structure and the latter can be explained by the "sinter-

Table 2
Surface area and pore properties of the raw Zn–Al and the calcined Zn–Al samples.

LDHs	Surface area (S_{BET}) (m^2/g)	Pore volume (cm^3/g)	Average pore size (nm)
Zn–Al	51.87	0.26	20.04
Zn–Al-150	62.58	0.31	15.09
Zn–Al-200	74.88	0.24	15.24
Zn–Al-300	81.20	0.15	12.10
Zn–Al-400	75.75	0.23	12.12
Zn–Al-500	63.97	0.28	21.12
Zn–Al-600	29.28	0.14	21.58

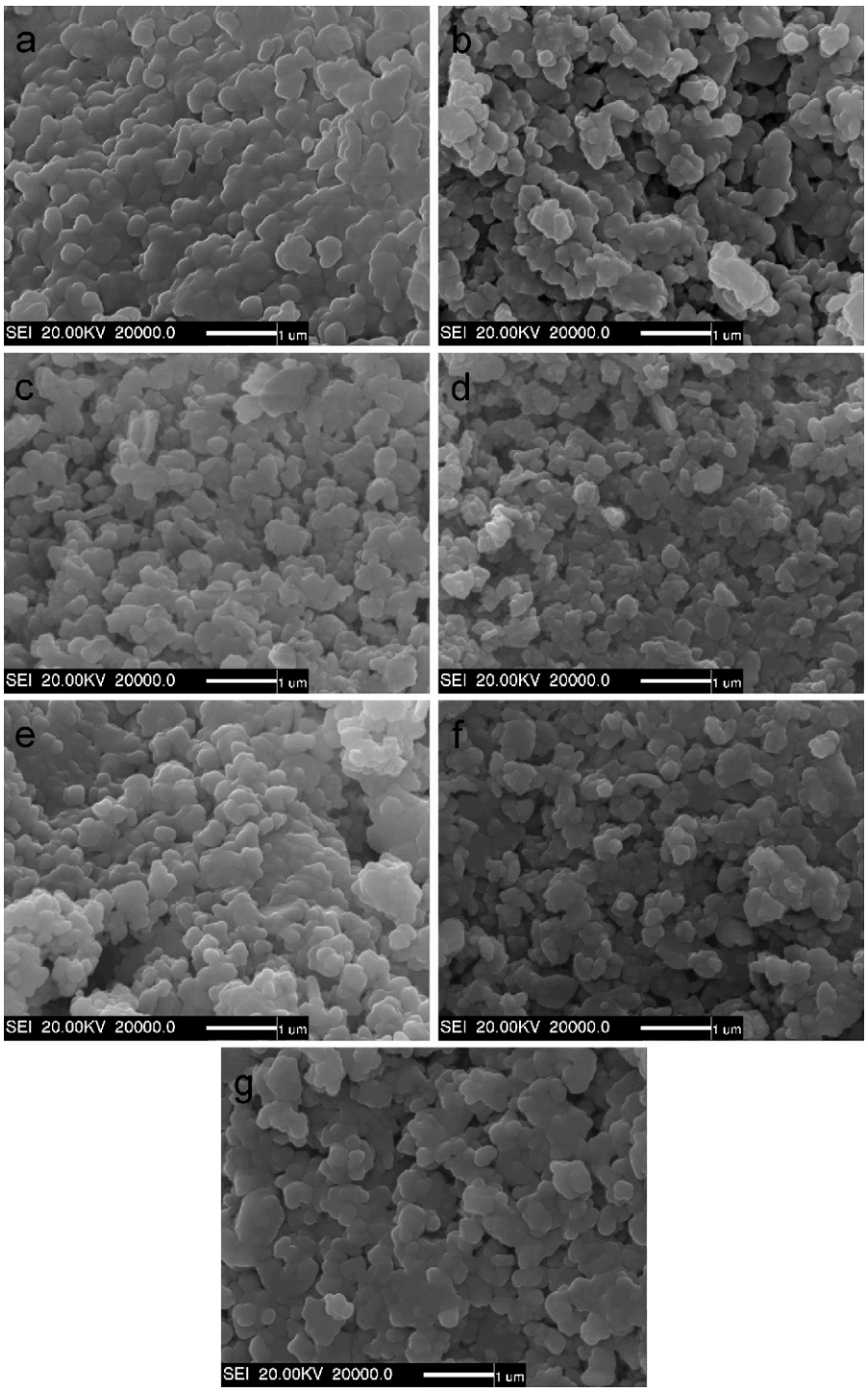

Fig. 4. SEM micrographs of the raw Zn–Al (a) and the Zn–Al calcined at 150 °C (b), 200 °C (c), 300 °C (d), 400 °C (e), 500 °C (f) and 600 °C (g).

ing" effect ($ZnAl_2O_4$ formation). The results are consistent with the phase change observed in the XRD analysis.

3.2. Phosphate adsorption by the LDHs

3.2.1. Calcination effect

As illustrated in Fig. 6, calcination treatment markedly improved phosphate adsorption by the Zn–Al LDHs with the temperature increasing to 300 °C. Phosphate uptake of 41.26 mg P/g was achieved by the Zn–Al-300 in 24 h, which was 1.52-fold higher than that of the raw LDHs. However, calcination at higher temperatures caused slight decreases in the P uptake. At 600 °C, a large drop in the P adsorption capacity of the sample was observed.

The observed variation in the phosphate adsorption capacity of the LDHs was closely related to their structural property dynamics during the calcination. The highest P uptake was achieved by Zn–Al-300, which exhibited the greatest specific surface area (Table 2). The result suggests that either the P uptake by the LDHs was partially attributed to the surface bonding in a physical adsorption or physical P sorption onto the solid surface promoted the entire P uptake by the Zn–Al LDHs or both. However, it had been found in our previous studies that CO_3^{2-} was much more efficient than Cl^-

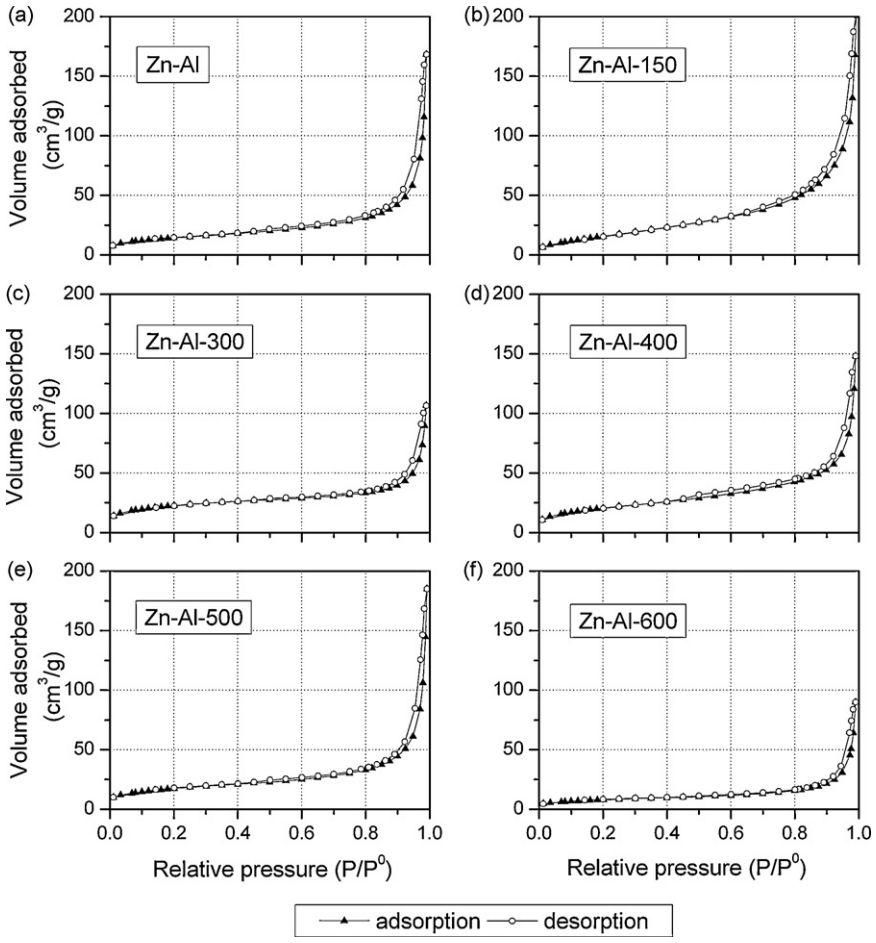

Fig. 5. N_2 adsorption–desorption isotherms of the raw Zn–Al and the calcined Zn–Al samples.

to desorb phosphate from the used Zn–Al-300 [26], indicating that the interaction between the LDHs and anions are selective. In other words, physical adsorption was not likely the main mechanism of P transfer onto the LDHs.

At calcination temperature of 300 °C, CO_3^{2-} was removed from the Zn–Al according to the FTIR spectra (Fig. 3). Many authors have reported that CO_3^{2-} is a major obstacle ion for anions removal by LDHs compounds [23,33]. Thus, the expulsion of the interlayer carbonate during the calcination could have contributed to the significant increase in P adsorption capacity of Zn–Al LDHs.

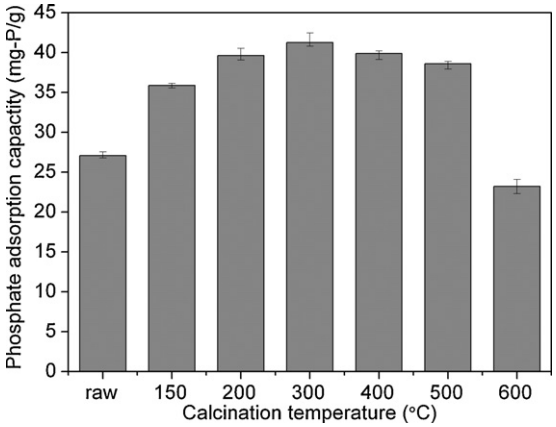

Fig. 6. Effect of calcination on the phosphate adsorption by Zn–Al LDHs from sludge liquor.

Many calcined LDHs will undergo a spontaneous rehydration (reconstruction) of the layered structure in an aqueous environment, which is called "Memory Effect" [21,30,34]. During this process, anion intercalation occurs, giving rise to a great increase in the adsorption capacity of the calcined LDHs compared with the precursor. In this work, the mineral phase of the sample evolved from LDHs to metal oxides and finally to spinel $ZnAl_2O_4$ with the calcination temperature increasing to 600 °C (Figs. 1 and 3). The high P adsorption by Zn–Al-300 can be due to the rehydration of the LDHs. The XRD pattern of the used Zn–Al-300 reveals that the LDHs structure was recovered (Fig. 1). In the FTIR spectrum of the used Zn–Al-300, the band at 1040 cm^{-1} (P in Fig. 3 can be assigned to the P–O stretching modes, indicating the phosphate was incorporated during the rehydration. The P adsorption capability of the LDHs fell dramatically when the Zn–Al was calcined at 600 °C. This can be explained by the facts: (1) the mineral transformed to the spinel $ZnAl_2O_4$ from a metastable phase of mixed metal oxides and (2) only a metaphase of metal oxides may reconstruct into the starting LDHs under appropriate conditions [35]. The phase change at 600 °C also led to a sharp decrease in the BET surface area (Table 2), which could have further weakened the P uptake by the Zn–Al-600.

3.2.2. Adsorption kinetics

Adsorption kinetics was tested by using the raw Zn–Al and the Zn–Al-300 samples for the purpose of determining the time required for adsorption equilibrium. According to Fig. 7a, the majority of the P uptake was completed in 24 h for both the raw Zn–Al (87%) and the Zn–Al-300 (91%). The phosphate adsorption equilibria were observed in approximately 72 h and the capaci-

Table 3
Kinetic constants for phosphate adsorption onto the raw Zn–Al and the Zn–Al-300 analyzed by pseudo-first-order, pseudo-second-order and Elovich models.

Model	Equation	Zn–Al		Zn–Al-300	
		Constant	R^2	Constant	R^2
Pseudo-first-order	$\frac{dq_t}{dt} = k_1(q_e - q)$	$q_e = 20.16$ $k_1 = 0.169$	0.972	$q_e = 34.60$ $k_1 = 0.165$	0.940
Pseudo-second-order	$\frac{dq_t}{dt} = k_2(q_e - q_t)^2$	$q_e = 31.64$ $k_2 = 0.018$	0.996	$q_e = 49.98$ $k_2 = 0.009$	0.997
Elovich	$\frac{dq_t}{dt} = \alpha \exp(-\beta q_t)$	$\alpha = 355.0$ $\beta = 0.292$	0.961	$\alpha = 113.9$ $\beta = 0.142$	0.974

q_e and q_t are the phosphate uptake (mg-p/L) at equilibrium and at time t (h), respectively. k_1 is the Lagergren rate constant of pseudo first-order adsorption (h^{-1}), k_2 is the equilibrium rate constant of pseudo second-order adsorption (g/mg h), α and β are constants of Elovich model.

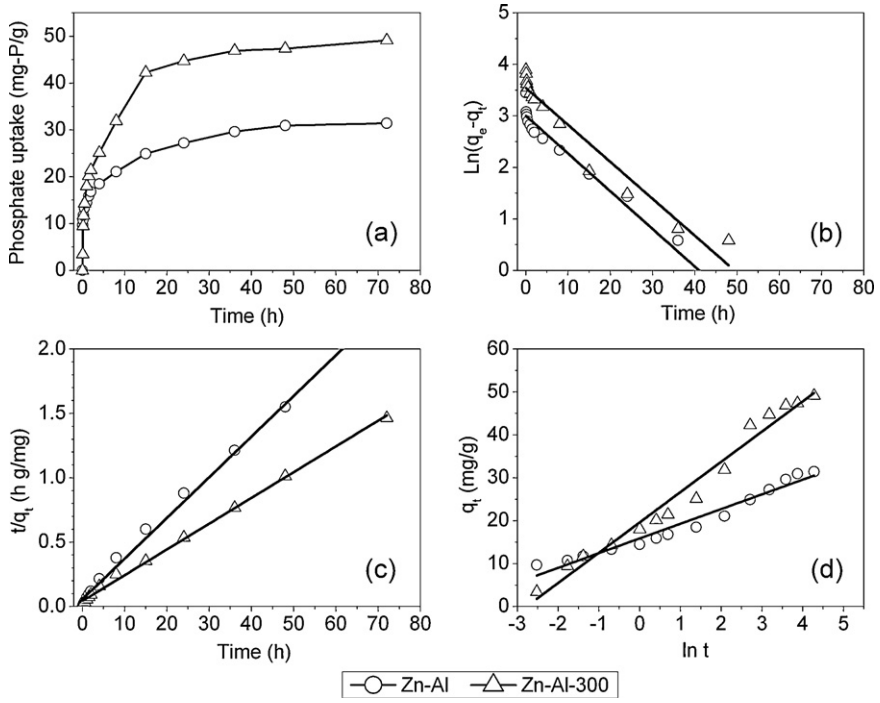

Fig. 7. Kinetics of the phosphate adsorption on the raw Zn–Al and the Zn–Al-300 from sludge liquor (a) and the data fitting by pseudo-first-order (b), pseudo-second-order (c) and Elovich (d) models.

ties were estimated as 31 and 50 mg P/g adsorbent, respectively. The experimental data were studied by pseudo-first-order [36], pseudo-second-order [37] and Elovich equations [38], and the results were shown in Fig. 7b–d and Table 3. The P adsorption by the Zn–Al and the Zn–Al-300 both followed pseudo-second-order kinetics the best with high correlation coefficients ($R^2 > 0.99$). The calculated P adsorption capacities at equilibria are 31.64 and 49.98 mg P/g, which closely agree with the tested values. Same type of kinetics was reported in previous studies of phosphate adsorption by many other materials, e.g., coir pith [39] and dolomite [40], and also of other anions adsorption by LDHs, e.g., fluoride [4].

3.2.3. Adsorption isotherms

Isotherms of phosphate adsorption on the raw and calcined Zn–Al samples were investigated to determine the adsorption capacities. The equilibrium experiments were carried out for a reaction period of 72 h based on the kinetic studies. The results are presented in Fig. 8. At the same equilibrium concentrations (especially when $C_e > 1$ mg/L), the P uptake of the Zn–Al-300 was much higher than that of the raw Zn–Al, indicating that the calcination effectively improved the phosphate adsorption capacity

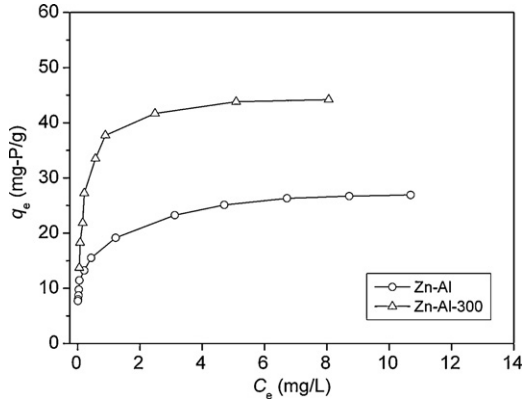

Fig. 8. Isotherms of phosphate adsorption onto the raw Zn–Al and the Zn–Al-300 from sludge liquor (adsorption temperature: 25 °C).

Table 4
Langmuir and Freundlich constants for phosphate adsorption onto the raw Zn–Al and the Zn–Al-300 from sludge liquor (adsorption temperature: 25 °C).

LDHs	Langmuir equation			Freundlich equation		
	q_m	b	R^2	K_f	n	R^2
Zn–Al	27.07	5.046	0.997	18.13	5.272	0.993
Zn–Al-300	45.02	6.382	0.999	32.84	4.540	0.874

of the Zn–Al LDHs. Langmuir and Freundlich models were used to study the P adsorption isotherms. The linear form of a Langmuir equation is shown as:

$$\frac{C_e}{q_e} = \frac{1}{bq_m} + \frac{C_e}{q_m} \quad (1)$$

where C_e (mg/L) is the phosphate equilibrium concentration, q_e (mg/g) denotes the amount of phosphate adsorbed per unit weight of LDHs at equlibrium, q_m (mg/g) is the maximum adsorption capacity for monolayer coverage and b (L/mg) is the Langmuir or binding coefficient. The logarithmic form of a Freundlich equation is represented as:

$$\ln q_e = \ln K_f + \frac{1}{n} \ln C_e \quad (2)$$

where C_e (mg/L) is the phosphate equilibrium concentration, q_e (mg/g) denotes the amount of phosphate adsorbed per unit weight of LDHs, and K_f and n are constants.

As illustrated in Table 4, the Langmuir equation yields better fits than the Freundlich equation for phosphate adsorption onto both the raw and calcined Zn–Al LDHs. According to the Langmuir modeling, the monolayer adsorption capacities of the Zn–Al and the Zn–Al-300 are evaluated to 27.07 and 45.02 mg P/g adsorbent respectively, which agree well with the experimental equilibrium capacities (26.9 and 44.2 mg P/g adsorbent, respectively). The higher b value for Zn–Al-300 indicates a steeper desirable beginning of the adsorption isotherm which reflects a higher affinity of the adsorbent for phosphate after calcination. The calculated values of n (>1) in the Freundlich equations indicate it was a favorable adsorption.

4. Conclusions

Calcination of Zn–Al LDHs was studied for the purpose of improving the phosphate adsorption from excess sludge liquor. During the calcination, the Zn–Al LDHs evolved to a phase of mixed metal oxides at 300 °C, and finally to spinel $ZnAl_2O_4$ at 600 °C. The highest phosphate uptake from the sludge liquor was achieved by the Zn–Al-300. The improvement in the phosphate adsorption capacity could be attributed to the physicochemical properties of the Zn–Al after being calcined at 300 °C: (1) the metastable mixed metal oxides which underwent a spontaneous rehydration of Zn–Al LDHs allowing phosphate incorporation as an interlayer anion; (2) the greatest surface area; and (3) the expulsion of the interlayer carbonate as a major obstacle anion. The phosphate adsorption by both the raw Zn–Al and the Zn–Al-300 samples followed a pseudo-second-order kinetic model. The obtained P adsorption isotherms for the raw Zn–Al and the Zn–Al-300 fit Langmuir-type equations well, but the latter showed a higher affinity for phosphate.

Based on the observations in this study, phosphate adsorption onto LDHs (raw or calcined) could be attributed to a combination of different mechanisms, e.g., surface adsorption, ion exchange and ion incorporation during the LDHs rehydration, etc. A more detailed investigation would be necessary to better understand the adsorption reactions at a microscopic scale and to further improve the adsorption capacity of LDHs as an efficient material for phosphorus recovery.

Acknowledgements

This work was supported by High-Tech Research and Development Program of China (863 Program, grant no. 2007AA06Z328) and National Eleventh Five-Year Research Program of China (grant no. 2006BAD03A0201).

References

[1] A. Monzón, N. Latorre, T. Ubieto, C. Royo, E. Romeo, J.I. Villacampa, L. Dussault, J.C. Dupin, C. Guimon, M. Montioux, Improvement of activity and stability of Ni-Mg-Al catalysts by Cu addition during hydrogen production by catalytic decomposition of methane, Catalysis Today 116 (2006) 264–270.
[2] R. Roto, A. Yamagishi, G. Villemure, Electrochemical quartz crystal microbalance study of mass transport in thin film of a redox active Ni–Al–Cl layered double hydroxide, Journal of Electroanalytical Chemistry 572 (2004) 101–108.
[3] D.P. Das, J. Das, K. Parida, Physicochemical characterization and adsorption behavior of calcined Zn/Al hydrotalcite-like compound (HTlc) towards removal of fluoride from aqueous solution, Journal of Colloid and Interface Science 261 (2003) 213–220.
[4] S. Mandal, S. Mayadevi, Adsorption of fluoride ions by Zn–Al layered double hydroxides, Applied Clay Science 40 (2008) 54–62.
[5] G. Carja, S. Ratoi, G. Ciobanu, I. Balasanian, Uptake of As (V) from aqueous solution by anionic clays type FeLDHs, Desalination 223 (2008) 243–248.
[6] S.H. Hwang, Y.S. Han, J.H. Choy, Intercalation of functional organic molecules with pharmaceutical, cosmeceutical and neutraceutical functions into layered double hydroxides and zinc basic salts, Bulletin-Korean Chemical Society 22 (2001) 1019–1022.
[7] T. Kwon, G.A. Tsigdinos, T.J. Pinnavaia, Pillaring of layered double hydroxides (LDH's) by polyoxometalate anions, Journal of the American Chemical Society 110 (1988) 3653–3654.
[8] D.W. Schindler, Evolution of phosphorus limitation in lakes, Science 195 (1977) 260–262.
[9] D.W. Schindler, Recent advances in the understanding and management of eutrophication, Limnology and Oceanography 51 (2006) 356–363.
[10] L.E. de-Bashan, Y. Bashan, Recent advances in removing phosphorus from wastewater and its future use as fertilizer (1997–2003), Water Research 38 (2004) 4222–4246.
[11] Y. Song, P. Yuan, B. Zheng, J. Peng, F. Yuan, Y. Gao, Nutrients removal and recovery by crystallization of magnesium ammonium phosphate from synthetic swine wastewater, Chemosphere 69 (2007) 319–324.
[12] T. Mino, M.C.M. Van Loosdrecht, J.J. Heijnen, Microbiology and biochemistry of the enhanced biological phosphate removal process, Water Research 32 (1998) 3193–3207.
[13] F.E. Dierberg, T.A. DeBusk, S.D. Jackson, M.J. Chimney, K. Pietro, Submerged aquatic vegetation-based treatment wetlands for removing phosphorus from agricultural runoff: response to hydraulic and nutrient loading, Water Research 36 (2002) 1409–1422.
[14] C. Namasivayam, D. Sangeetha, Equilibrium and kinetic studies of adsorption of phosphate onto $ZnCl_2$ activated coir pith carbon, Journal of Colloid and Interface Science 280 (2004) 359–365.
[15] B. Kostura, H. Kulveitová, J. Leško, Blast furnace slags as sorbents of phosphate from water solutions, Water Research 39 (2005) 1795–1802.
[16] Y. Seida, Y. Nakano, Removal of phosphate by layered double hydroxides containing iron, Water Research 36 (2002) 1306–1312.
[17] A. Ler, R. Stanforth, Evidence for surface precipitation of phosphate on goethite, Environmental Science & Technology 37 (2003) 2694–2700.
[18] R. Chitrakar, S. Tezuka, A. Sonoda, K. Sakane, K. Ooi, T. Hirotsu, Selective adsorption of phosphate from seawater and wastewater by amorphous zirconium hydroxide, Journal of Colloid and Interface Science 297 (2006) 426–433.
[19] D. Zhao, K. Sengupta, Selective removal and recovery of phosphate in a novel fixedbed process, Water Science and Technology 33 (1996) 139–147.
[20] K. Kuzawa, Y.J. Jung, Y. Kiso, T. Yamada, M. Nagai, T.G. Lee, Phosphate removal and recovery with a synthetic hydrotalcite as an adsorbent, Chemosphere 62 (2006) 45–52.
[21] J. Das, B.S. Patra, N. Baliarsingh, K.M. Parida, Adsorption of phosphate by layered double hydroxides in aqueous solutions, Applied Clay Science 32 (2006) 252–260.
[22] R. Frost, A. Musumeci, T. Kloprogge, M. Adebajo, W. Martens, Raman spectroscopy of hydrotalcites with phosphate in the interlayer-implications for the removal of phosphate from water, Journal of Raman Spectroscopy 37 (2006) 733–741.
[23] H.S. Shin, M.J. Kim, S.Y. Nam, H.C. Moon, Phosphorus removal by hydrotalcite-like compounds (HTLcs), Water Science and Technology 34 (1996) 161–168.
[24] M. Badreddine, A. Legrouri, A. Barroug, A. De Roy, J.P. Besse, Ion exchange of different phosphate ions into the zinc-aluminium-chloride layered double hydroxide, Materials Letters 38 (1999) 391–395.
[25] R. Chitrakar, S. Tezuka, A. Sonoda, K. Sakane, K. Ooi, T. Hirotsu, Adsorption of phosphate from seawater on calcined MgMn-layered double hydroxides, Journal of Colloid and Interface Science 290 (2005) 45–51.
[26] X. Cheng, X. Huang, X. Wang, B. Zhao, A. Chen, D. Sun, Phosphate adsorption from sewage sludge filtrate using zinc–aluminum layered double hydroxides, Journal of Hazardous Materials 169 (2009) 958–964.

[27] K.-H. Goh, T.-T. Lim, Z. Dong, Application of layered double hydroxides for removal of oxyanions: a review, Water Research 42 (2008) 1343–1368.
[28] A.P.H.A., A.W.W.A., W.E.F., Standard Methods for the Examination of Water and Wastewater, 20th ed., American Public Health Association, Washington, DC, 1998.
[29] W. Yang, Y. Kim, P.K.T. Liu, M. Sahimi, T.T. Tsotsis, A study by in situ techniques of the thermal evolution of the structure of a Mg–Al–CO_3 layered double hydroxide, Chemical Engineering Science 57 (2002) 2945–2953.
[30] O.P. Ferreira, O.L. Alves, D.X. Gouveia, A.G. Souza Filho, J.A.C. de Paiva, J.M. Filho, Thermal decomposition and structural reconstruction effect on Mg–Fe-based hydrotalcite compounds, Journal of Solid State Chemistry 177 (2004) 3058–3069.
[31] J.M. Fernández, M.A. Ulibarri, F.M. Labajos, V. Rives, The effect of iron on the crystalline phases formed upon thermal decomposition of Mg–Al–Fe hydrotalcites, Journal of Materials Chemistry 8 (1998) 2507–2514.
[32] K.S.W. Sing, D.H. Everett, R.A.W. Haul, L. Moscou, R.A. Pierotti, J. Rouquerol, T. Siemieniewska, Reporting physisorption data for gas/solid systems with special reference to the determination of surface area and porosity, Pure and Applied Chemistry 57 (1985) 603–619.
[33] G.P. Gillman, A simple technology for arsenic removal from drinking water using hydrotalcite, Science of the Total Environment 366 (2006) 926–931.
[34] L. Châtelet, J.Y. Bottero, J. Yvon, A. Bouchelaghem, Competition between monovalent and divalent anions for calcined and uncalcined hydrotalcite: anion exchange and adsorption sites, Colloids and Surfaces A: Physicochemical and Engineering Aspects 111 (1996) 167–175.
[35] T.S. Stanimirova, I. Vergilov, G. Kirov, N. Petrova, Thermal decomposition products of hydrotalcite-like compounds: low-temperature metaphases, Journal of Materials Science 34 (1999) 4153–4161.
[36] S. Lagergren, About the theory of so-called adsorption of soluble substance, Kungliga svenska vertenskapsakademiens, Hand linger 24 (1898) 1–39.
[37] Y.S. Ho, G. McKay, Pseudo-second order model for sorption processes, Process Biochem. 34 (1999) 451–465.
[38] C. Aharoni, D.L. Sparks, S. Levinson, I. Ravina, Kinetics of soil chemical reactions: relationships between empirical equations and diffusion models, Soil Science Society of American Journal 55 (1991) 1307–1313.
[39] K.A. Krishnan, A. Haridas, Removal of phosphate from aqueous solutions and sewage using natural and surface modified coir pith, Journal of Hazardous Materials 152 (2008) 527–535.
[40] S. Karaca, A. Gürses, M. Ejder, M. Açıkyıldız, Kinetic modeling of liquid-phase adsorption of phosphate on dolomite, Journal of Colloid and Interface Science 277 (2004) 257–263.